TECHNICAL ARTICLE

Effect of Copper Addition on the Formability of 304L Austenitic Stainless Steel

Ali Huang, Keping Wang, Yangyang Zhao, Wurong Wang, Xicheng Wei, and Jingguang Peng

To improve the antibacterial properties of 304L austenitic stainless steel, copper is often added as an antibacterial agent, but the forming performance of the resulting material is poor, impacting its actual production and use. Therefore, this study investigated the influence of copper addition on the formability of 304L austenitic stainless steel with drawing, cupping and conical cup forming tests. Mechanical properties were determined with tensile and hardness tests. The microstructure and phase transformation were further characterized by metallographic microscopy, scanning electron microscopy and x-ray diffraction analysis. It was found that the addition of copper impaired the mechanical properties of 304L austenitic stainless steel, increased the stacking fault energy of the material and inhibited the occurrence of strain-induced martensite transformation, leading to a decrease in the formability of 304L austenitic stainless steel.

1. Introduction

Stainless steel has been widely used in schools, restaurants, transportations and other public areas because of its excellent combination of good mechanical properties, reliable chemical stability and outstanding decorative functions (Ref 1-3). With increasing attention given by society to health and hygiene awareness, more stringent requirements for the performance of stainless steel materials have been put forward. Copper ions released from the surface of the copper-containing materials endow the material with a broad spectrum of antibacterial activities. It shows strong inactivation of common infectious bacteria such as Escherichia coli and Staphylococcus aureus (Ref 4). Severe acute respiratory syndrome coronavirus 2 (SARS-CoV-2) shows strong stability on the surface of conventional stainless steel, and even after three days, infectious virus can be detected, posing a high risk of virus transmission through surface contact in public places (Ref 5). The developed anti-pathogen stainless steel containing 20% copper can significantly reduce its surface-active SARS-CoV-2 by 99.99% within 6 h (Ref 6). In addition, copper is a trace element needed by human body, which can promote the synthesis of human hemoglobin and effectively reduce the

apoptosis rate of cells (Ref 7, 8). Therefore, the research and development of new stainless steel materials with antibacterial and antiviral functions has become the next important goal of the developers of antibacterial stainless steel containing copper.

In metastable austenitic steels, deformation mechanisms, including deformation-induced plasticity (TRIP) and twinning-induced plasticity (TWIP), are generally determined by the stacking fault energy (SFE), which is sensitively affected by its composition (Ref 9). Copper is an SFE-increasing element (Ref 10). Choi and coworkers (Ref 11) added 1 wt.% copper into an austenitic high-Mn TRIP steel, and the tensile properties were improved when TRIP and TWIP were well homogenized. However, a high addition of copper could suppress the formation of martensite and improve the amount of deformation twins after tensile deformation, in accordance with the SFE (Ref 12). Gonzalez et al. (Ref 13) investigated the effect of copper on the formability of austenitic stainless steel. The results showed that the addition of copper suppressed ε-martensite formation and decreased the kinetics of α′-martensite formation. Both uniform elongation and total elongation were improved by the decrease in the strain hardening rate due to the addition of copper. The ultimate tensile strength increases with higher copper concentrations until alloying with 5.5% copper, at which point it remains constant (Ref 14). The mechanical properties of austenitic steels also depend strongly on the stability of the matrix. Copper is also an austenite stabilizer (Ref 10). According to the research conducted by Kim et al. (Ref 15), the volume of retained austenite increased with the addition of copper, as the increased austenite stability resulted in both a higher strength and a higher ductility.

Copper usually remains either in solution or as nanoprecipitates in steels. Precipitation of the copper-rich phase will occur upon aging treatment, and copper-rich precipitation is one of the most effective intermetallic strengthening precipitates (Ref 16). Because of the slower diffusion kinetics of copper, low interfacial energy and high strain energy of copper-rich precipitates in the austenite matrix, copper-rich precipitates grow and coarsen slowly, which is consistent with the modest

Ali Huang, Keping Wang, Yangyang Zhao, Wurong Wang, Xicheng Wei, and Jingguang Peng, School of Materials Science and Engineering, Shanghai University, Shanghai, People's Republic of China; and State Key Laboratory of Advanced Special Steel, Shanghai University, Rm 425 Material Building C, 333 Nanchen Road, Shanghai 200444, People's Republic of China. Contact e-mail: pengjg@shu.edu.cn.

change in hardness and yield strength with extended aging (Ref 17). Yang et al. (Ref 18) thought that this fine precipitate improved the strength and maintained the plasticity of the material. Small additions of copper will not have adverse effects on the fracture and fatigue behavior of the stainless resulting steel (Ref 19).

In this paper, 304L austenitic stainless steel was treated with more than 3.5% copper, and only solution treatment was used; this resulted in an excellent antibacterial effect. However, this kind of material easily cracks during the forming process and has poor forming performance, which greatly limits its application range. Since copper affects the microstructural and mechanical properties of steel, which may further affect its formability, this study started from practical problems, conducted an in-depth study on the poor formability of this copper-containing austenitic antibacterial stainless steel and determined the influence of copper addition on the formability of 304L austenitic stainless steel.

2. Materials and Methods

The billet was heated to 1250 °C in a walking beam furnace and then rolled into a steel strip with a thickness of 3.0 mm. First, the steel strip was held at 1150 °C for 10 min for solution treatment and then cold rolled into a 0.8 mm cold rolled steel strip many times. Finally, the cold rolled steel strip was held at 1050 °C for 10 min and then pickled to obtain the experimental steel sheet. The chemical compositions of the two experimental steels used in this work are listed in Table 1. The contents of Cr, Ni and other elements in the two materials were similar, while the content of Cu in 304L-Cu was 4.01%.

At room temperature, deep drawing, cupping and conical cup forming tests were performed with a Zwick BUP-600 sheet metal forming tester according to GB/T15825.3-2008 "Sheet metal formability and test methods", and the rising speed of the punch was 1 mm/s.

The limiting drawing ratio (LDR) was measured with a deep drawing test. The diameter difference of two adjacent samples was 1.25 mm, and there were six valid samples in each group. The method of increasing the sample diameter step by step was used to measure the maximum allowable diameter of the wall near the bottom fillet of the drawing cup without breakage. In a group of samples, when three samples were broken, three samples were not broken, or when the number of broken samples of a certain grade was less than 3 and the diameter increased by one grade, the number of broken samples was greater than or equal to 4, and the experiment was stopped.

$$\mathrm{LDR} = \frac{(D_0)_{\max}}{d_p} \qquad (\mathrm{Eq}\ 1)$$

where $(D_0)_{\max}$ is the maximum diameter that can be punched out of a cup shape without damage and d_p is the punch diameter of 50 mm. The higher the LDR is, the better the drawability of the sheet metal.

The samples used for the cupping tests were 100×100 mm thin square sheets. The Erichsen index (IE) is the dent depth measured by displacement of the punch, which was measured six times and averaged. The larger the IE was, the better the bulging performance of the sheet metal.

The diameter of the conical cup test sample was 36 mm, and the conical cup was formed by a spherical punch until the sidewall at the bottom of the cup broke. The distance between the peaks of two opposite lugs at the mouth of the conical cup was measured as the maximum outer diameter ($\overline{D}_{\max}$), and the distance between the valleys was measured as the minimum outer diameter ($\overline{D}_{\min}$). The conical cup value (CCV) was obtained according to Eq 2. The smaller the CCV is, the better the "drawing + bulging" composite performance of the sheet metal.

$$\mathrm{CCV} = \overline{D}_{\max} + \overline{D}_{\min} \qquad (\mathrm{Eq}\ 2)$$

According to GB/T 228.1-2010, an MTS tensile test machine was used to carry out tensile tests on the 304L and 304L-Cu samples at 0, 45 and 90° to the rolling direction. The tensile rate was 3 mm/min.

The microstructures of the samples before and after tensile testing were observed with a Nikon LV150NL vertical metallographic microscope. The hardness was measured on a Hengyi MH-3 L Micro Vickers Hardness Tester at six different points on the sample surface, and the average was used for the hardness value.

Phases were examined with a Japan D/max-2550 x-ray diffractometer (Cu -Kα radiation). The maximum rated power was 18 kW, and the speed was 6°/min. The volume fraction of martensite was quantified with the following equation:

$$V_{\alpha'} = \frac{\frac{1}{n}\sum_{j=1}^{n} \frac{I_{\alpha'}^{j}}{R_{\alpha'}^{j}}}{\frac{1}{n}\sum_{j=1}^{n} \frac{I_{\alpha'}^{j}}{R_{\alpha'}^{j}} + \frac{1}{n}\sum_{j=1}^{n} \frac{I_{\gamma}^{j}}{R_{\gamma}^{j}}} \qquad (\mathrm{Eq}\ 3)$$

where n is the number of peaks examined, I is the integrated intensity and R is the material scattering factor. The integrated intensities of the $(200)\gamma$, $(220)\gamma$, $(311)\gamma$, $(200)\alpha'$ and $(211)\alpha'$ peaks were used to calculate the volume fraction of the phase.

The tensile fracture morphology was observed with a ZEISS Sigma 300 SEM to determine the fracture mechanism.

3. Results

3.1 Formability

The results of the drawing experiments are shown in Fig. 1, and the details are shown in Table 2. When the diameter was small, both 304L and 304L-Cu samples could be punched out

Table 1 Chemical compositions of the experimental steels (mass fraction, %)

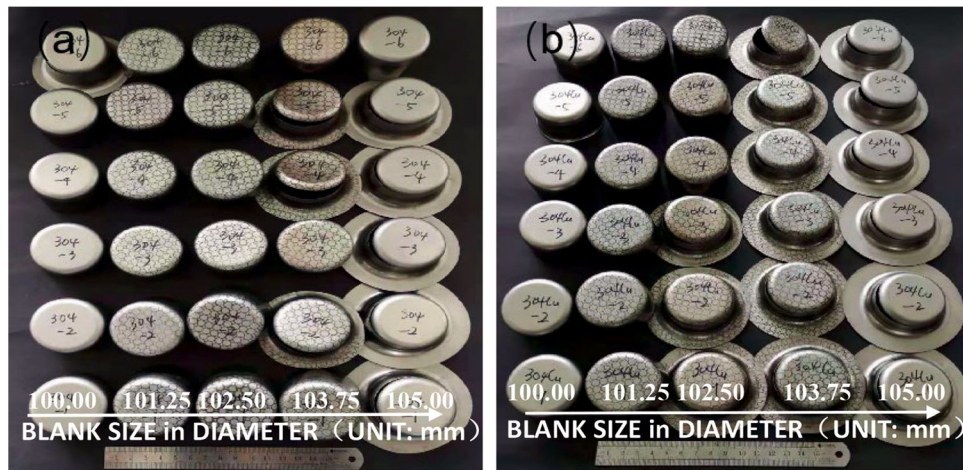| Steel	C	Si	Mn	P	S	N	Cr	Ni	Cu	Fe
304L	0.017	0.354	1.120	0.018	< 0.001	0.077	17.99	7.85	0.18	Bal.
304L-Cu	0.015	0.361	1.025	0.021	0.001	0.056	17.77	7.85	4.01	Bal.

Fig. 1 Samples after the drawing tests: (a) 304L and (b) 304L-Cu

Table 2 Deep drawing test results for 304L and 304L-Cu samples

Steel	Diameter, mm	Broken number	Unbroken number
304L	100.00	1	5
	101.25	0	6
	102.50	0	6
	103.75	3	3
	105.00	5	1
304L-Cu	100.00	0	6
	101.25	0	6
	102.50	3	3
	103.75	6	0
	105.00	6	0

Table 3 LDRs of 304L and 304L-Cu

Steel	304L	304L-Cu
$(D_0)_{max}$/mm	103.75	102.50
LDR	2.08	2.05

to form complete cups. When the diameter was increased to 102.50 mm, six of the 304L samples still showed good drawing performance, while half of the 304L-Cu samples failed. When the diameter was increased to 103.75 mm, all 304L-Cu samples were broken, and half of the 304L samples were also broken.

In a group, the diameter can be regarded as the maximum diameter when the number of broken and unbroken samples is equal. The maximum diameters of 304L and 304L-Cu samples were 103.75 and 102.50 mm, respectively. According to Eq 1, the LDRs of 304L and 304L-Cu were 2.08 and 2.05, respectively, as shown in Table 3.

The LDR value of 304L was slightly higher than that of 304L-Cu, indicating that the drawing performance of 304L was moderately better than that of 304L-Cu.

Table 4 shows the cupping test results for 304L and 304L-Cu. The cupping values of 304L were greater than 12 mm in six measurements, while those of 304L-Cu fluctuated at approximately 11 mm. Finally, the $IE_{Aver.}$ of 304L was

Table 4 Cupping value IEs (mm) of 304L and 304L-Cu

Number	304L	304L-Cu
1	12.54	11.25
2	12.88	10.93
3	12.69	11.30
4	12.93	11.04
5	12.36	11.30
6	12.75	11.13
$IE_{Aver.}$	12.69	11.16

1.53 mm higher than that of 304L-Cu. The bulging performance of 304L was better than that of 304L-Cu. Cracks appeared on the surfaces of 304L and 304L-Cu samples after the cupping tests (as shown in Fig. 2).

The experimental results for the conical cup test are shown in Table 5. The $CCV_{Aver.}$ values for 304L and 304L-Cu were 38.2 and 38.5 mm, respectively; the CCV of 304L-Cu was slightly higher, which indicated that its "drawing + bulging" composite performance was slightly worse. Figure 3 shows the sample morphologies after conical cup tests.

With the addition of copper, the drawing and bulging performance of 304L decreased to varying degrees, the drawing diameter decreased by one level, and the cupping value decreased by 12%, which led to a decline in the "drawing + bulging" composite performance of 304L-Cu in the conical cup tests. This was not conducive to the production of cup-shaped parts in practical applications.

3.2 Microstructure

Figure 4(a) and (b) show the original microstructure metallographic diagrams of 304L and 304L-Cu, which showed austenite without deformation, but the grain sizes were nonhomogeneous and consisted of large grains surrounded by many subgrains. This was because deformation-induced martensite (DIM) formed reversion-refined fine grains, and detained austenite (DA) formed recrystallized grains, as discussed in several papers (Ref 16, 17). The average grain size for 304L was 32 μm (for GS ASTM #7), and that for 304L-Cu was 23 μm (for GS ASTM #8.5).
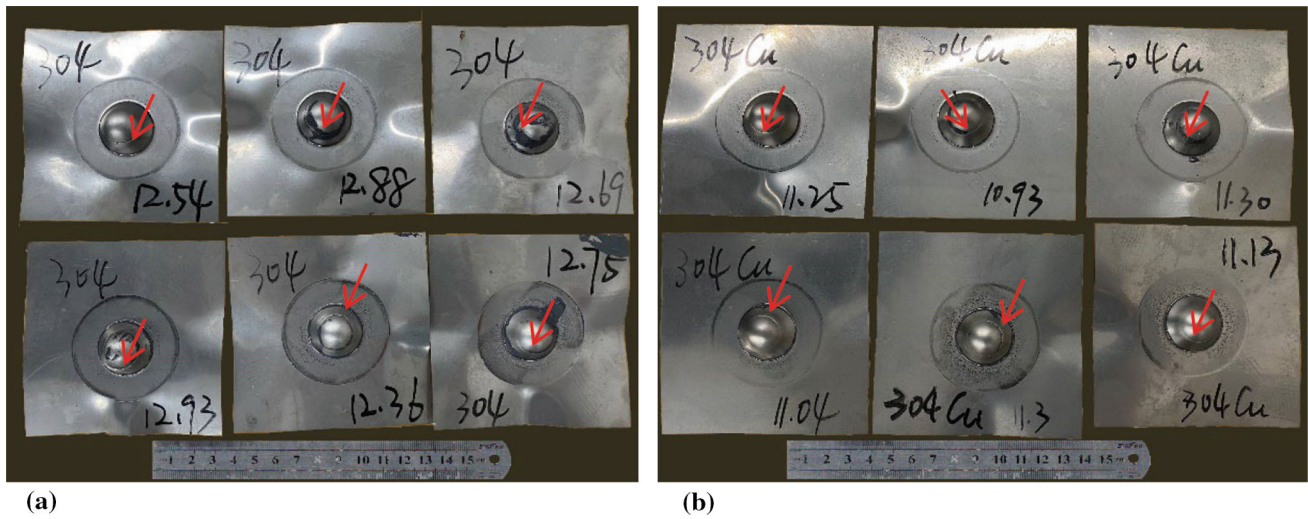
Fig. 2 Samples after the cupping tests: (a) 304L and (b) 304L-Cu (the position indicated by the red arrow is where a crack is located)

Table 5 CCVs (mm) of 304L and 304L-Cu

Number	304L		304L-Cu	
	$\overline{D}_{max}$	$\overline{D}_{min}$	$\overline{D}_{max}$	$\overline{D}_{min}$
1	38.7	37.8	38.2	38.2
2	38.2	37.6	38.5	38.2
3	38.7	37.9	38.8	38.5
4	38.7	37.9	38.7	38.4
5	38.1	38.6	38.4	38.2
6	38.3	37.4	38.9	38.5
CCV$_{Aver}$	38.2	38.5		

Figure 4(c) and (d) show the microstructure diagrams of 304L and 304L-Cu after tensile testing. Upon undergoing plastic deformation, the austenite grains of 304L and 304L-Cu deformed along the tensile direction, and the deformation degree of 304L grains was greater. In addition, dark lath martensite was found on the 304L matrix but not on the 304L-Cu matrix.

3.3 Mechanical Properties

The basic mechanical properties of 304L and 304L-Cu were obtained with tensile tests. Figure 5 shows the engineering stress–strain curves for both steels. Table 6 lists detailed mechanical properties, including yield strength (YS), ultimate
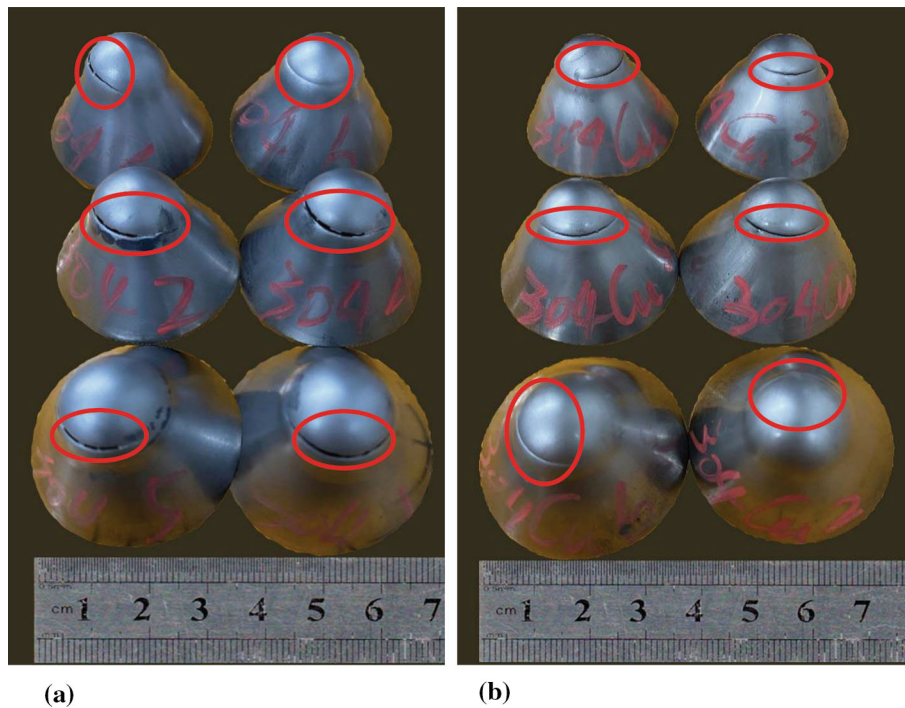

Fig. 3 Samples after conical cup tests: (a) 304L and (b) 304L-Cu (the red circles show where cracks are located)
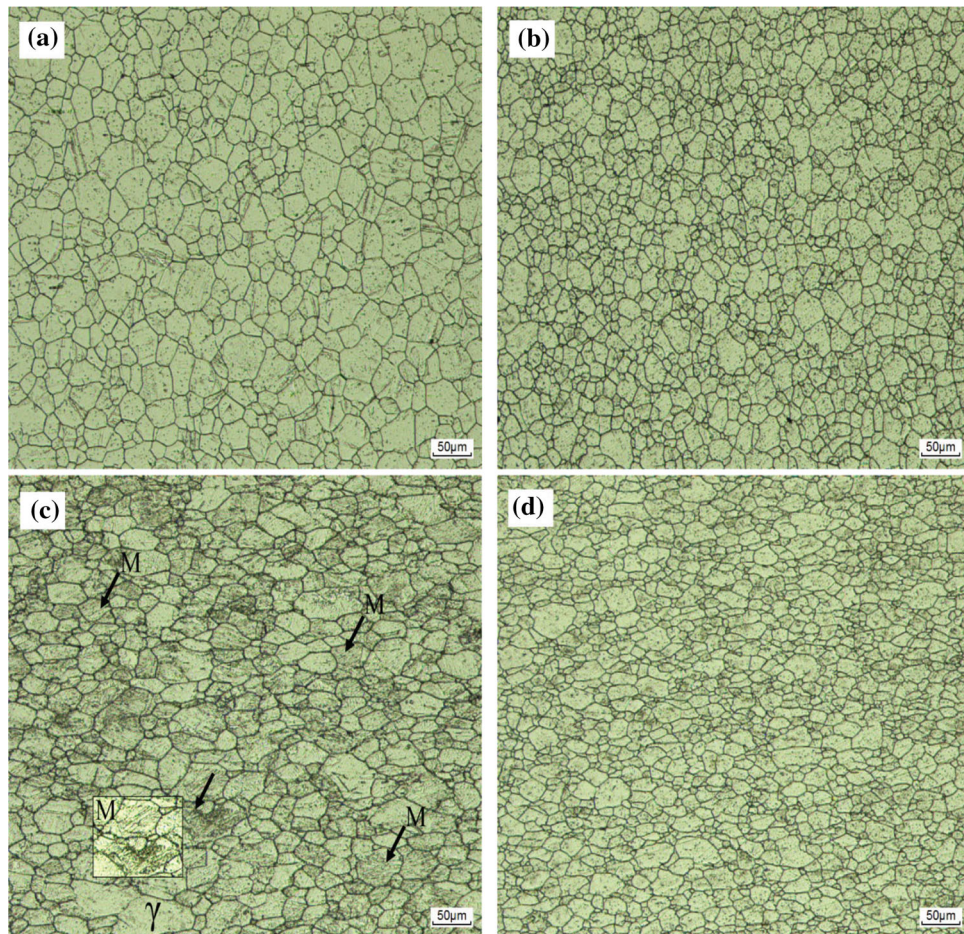
Fig. 4 Microstructure diagrams: (a) 304L original sample, (b) 304L-Cu original sample, (c) 304L tensile sample and (d) 304L-Cu tensile sample
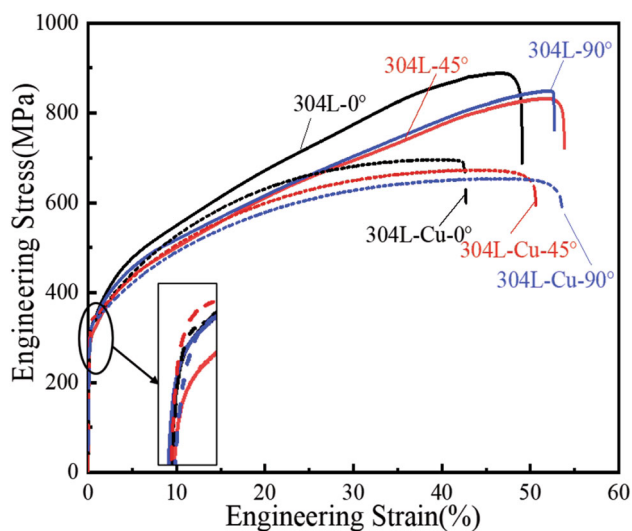

Fig. 5 Engineering stress–strain curves of 304L and 304L-Cu

tensile strength (UTS), yield ratio (YS/UTS), elongation (EL), strain hardening index (n) and plastic strain ratio (r). Both 304L and 304L-Cu showed different mechanical properties at 0°, 45° and 90°, as shown in Fig. 6. 304L demonstrated the highest YS of 322 MPa and the lowest UTS of 835 MPa, while the lowest

YS and highest UTS for 304L-Cu were 322 and 696 MPa, respectively, from which we can conclude that 304L-Cu had higher YS values and lower UTS values than 304L, so the yield ratios of 304L-Cu were higher. The elongations of 304L-Cu decreased slightly, but they remained at approximately 50%. Additionally, after adding copper, the strain hardening index n and the plastic strain ratio r decreased to varying degrees. Generally, almost all property parameters were worsened with copper addition, and it is worth mentioning that the difference in mechanical properties of 304L-Cu became more obvious.

The fractographs of 304L and 304L-Cu obtained after tensile testing are shown in Fig. 6. Large numbers of dimples and very small holes were evenly distributed on the fracture surfaces of both steels, indicating a typical ductile fracture mechanism, so they both showed high elongation in the tensile tests. Moreover, obvious necking was seen on the fracture surface. These figures revealed that the addition of copper had little effect on the fracture mechanism of the material.

The hardness values of 304L and 304L-Cu steels are given in Table 7. The initial hardness values of 304L and 304L-Cu were 208 HV and 221 HV, respectively. The hardness of 304L-Cu was 6.2% higher than that of 304L. The addition of copper improved the hardness of 304L. After tensile deformation, the hardness values of 304L and 304L-Cu increased, but the hardness of 304L was significantly higher than that of 304L-Cu.

Table 6   Mechanical properties of 304L and 304L-Cu at room temperature

Steel	Direction, °	YS, MPa	UTS, MPa	YS/UTS	EL, %	*n*	*r*
304L	0	322	889	0.36	51	0.304	0.855
	45	301	835	0.36	53	0.279	0.782
	90	318	849	0.37	53	0.274	0.701
304L-Cu	0	329	696	0.47	42	0.270	0.760
	45	340	680	0.50	49	0.260	0.824
	90	322	649	0.50	53	0.249	0.611
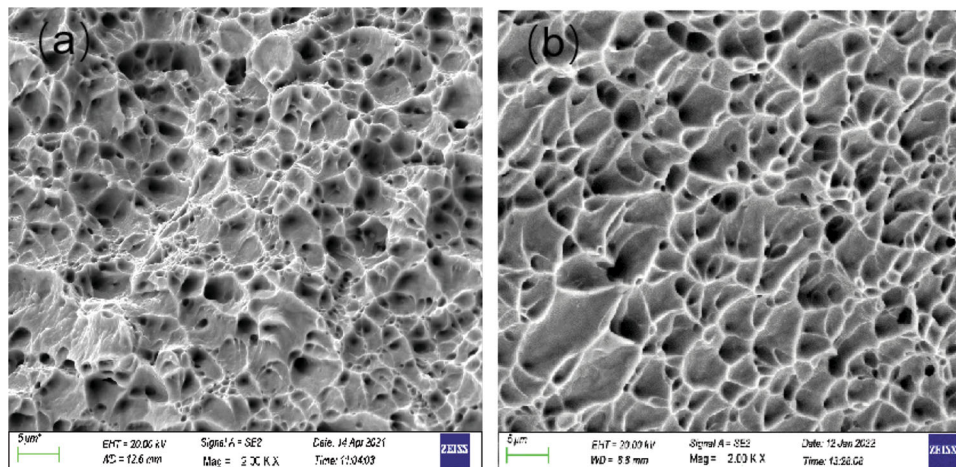
Fig. 6   Tensile fracture morphologies: (a) 304L and (b) 304L-Cu

Table 7   Hardness test results

Steel	Initial hardness/HV	Tensile hardness/HV
304L	208	364
304L-Cu	221	288

3.4 XRD Studies

X-ray diffraction (XRD) analyses were performed with 304L and 304L-Cu samples before and after tensile testing, as shown in Fig. 7. The intensities of the martensite diffraction peaks for 304L and 304L-Cu increased after tensile deformation, while those of the austenite diffraction peaks decreased, implying the formation of martensite. There was some martensite present in 304L prior to testing, as indicated by the weak martensite peak appearing in the sample, while the microstructure of 304L-Cu was almost fully composed of austenite. The higher peak intensity for (211)α' in 304L suggested that more martensite was formed during the tension than was the case for 304L-Cu. As copper was added to a level of 4.01 wt.%, the formation of martensite was effectively suppressed.

4. Analysis and Discussion

4.1 Effect of Copper Addition on Strain-Induced Martensitic Transformation

The microstructures of 304L and 304L-Cu after solution treatment indicated metastable austenite, which transforms to martensite during plastic deformation at room temperature, namely, strain-induced martensite. Strain-induced martensite has two different crystalline structures. The first is ε-martensite with a hexagonal close-packed structure, which is paramagnetic. The other is α'-martensite with a body-centered cubic structure, which is magnetic (Ref 20). No obvious diffraction peaks for the ε phase were detected in any of the samples, indicating that little ε-martensite existed in both steels. These results agree with those of Huang et al. (Ref 21) and Choi et al. (Ref 22).

SFE is an important parameter that influences the amount of martensite formed (Ref 23). According to the method reported by Curtze et al. (Ref 24), the SFEs of 304L and 304L-Cu were 23.69 and 27.41 MJ/m^2, respectively. The SFE value for 304L-Cu was higher than that for 304L by approximately 4 MJ/m^2 due to the addition of copper. The volume fractions of transformed martensite for 304L and 304L-Cu after tensile deformation were 28.75% and 9.43%, respectively. There were larger quantities of α'-martensite formed in 304L than in 304L-Cu, and the value for 304L was about three times that for 304L-Cu. SFE affects the frequency of intersection between mechanical twins, which act as nucleation sites for α'-martensite (Ref 22). Additionally, as reported by Venables (Ref 25), the stress required for twinning deformation is parabolically proportional to the SFE. Therefore, 304L with a lower SFE more easily formed mechanical twins than 304L-Cu, so 304L formed a larger amount of α'-martensite than 304L-Cu. A high copper content promoted an increase in SFE, thus inhibiting the formation of magnetic martensite nucleation sites (Ref 26). Therefore, little martensite was found on the 304L-Cu matrix after plastic deformation (Fig. 4d).
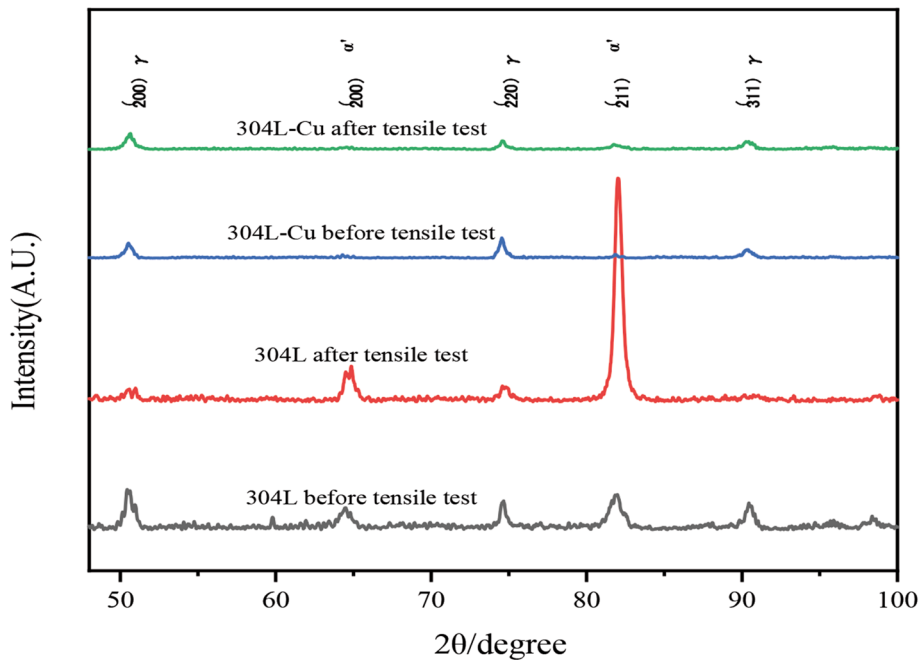
Fig. 7 XRD patterns of 304L and 304L-Cu

A higher SFE for 304L-Cu means that the austenite was more stable; therefore, it should have a lower M_{d30} (the temperature at which 50% martensite is formed at a plastic strain of 30%) than 304L. According to the following empirical equation proposed by Nohara et al. (Ref 27), $M_{d30}(°C) = 552-462(C\% + N\%)-9.2Si\%-8.1Mn\%-13.7Cr\%-29.0(Ni\% + Cu\%)-18.5Mo\%-68.0Nb\%-1.42(GS-8)$, where GS is the ASTM grain size and the M_{d30} values of 304L and 304L-Cu were 18.2 and −80.5 °C, respectively. Copper alloying increased the stability of the steel by increasing the SFE and decreasing M_{d30}.

The strain hardening behavior of metastable austenite depends on the state of the strain-induced martensite (Ref 28), which is strongly related to the SFE. The hardness of martensite is much higher than that of austenite. Rapid accumulation in a short time leads to a great increase in the hardness of a material, resulting in strain hardening. The hardness values of 304L and 304L-Cu were increased by 75% and 30%, respectively. The increased hardness was consistent with the martensite transformation.

4.2 Effect of Copper Addition on Mechanical Properties

With the addition of copper, the grain sizes of 304L were reduced by 28%. The grains were obviously refined, which is consistent with the results of previous studies (Ref 29, 30). According to the Hall–Petch formula, the finer the polycrystalline grains of metal are, the higher the yield strength of the material, so the yield strength of 304L-Cu was higher than that of 304L. The formation of a smaller amount of martensite led to a decrease in the strain hardening rate of the steel containing copper, resulting in a decrease in the maximum uniform elongation of 304L-Cu and deterioration of the UTS values. The yield ratio increased, and the uniform deformation ability decreased, from which we concluded that adding copper impaired the mechanical properties of the steel.

4.3 Effect of Copper Addition on Formability

The enhanced formability of steels undergoing strain-induced martensitic transformation is associated with high uniform elongation. When copper is added, the martensite transformation is inhibited and cannot promote deformation dispersion. This led to a lower uniform strain and decreases in the n value and r value. The greater the value of n is, the better the uniform deformation and formability of the material. The larger the value of r is, the stronger the thinning resistance in the thickness direction and the better the drawing performance of the material. Consequently, the 304L-Cu exhibited a worse stretch formability than the 304L, as measured with the LDR, IE and CCV metrics.

5. Conclusions

(1) The addition of copper improved the yield strength and yield ratio, increased the deformation resistance and decreased the uniform elongation of 304L austenitic stainless steel. During the forming process, the material easily cracked, which is not conducive to forming.

(2) Adding copper increased the stability of 304L by increasing its SFE and decreasing the M_{d30} temperature, which led to inhibition of strain-induced martensitic transformation and decreases in the strain hardening index n and the plastic strain ratio r.

(3) After copper was added, the LDR and IE decreased, the CCV increased, and the "drawing + bulging" performance decreased, which indicated that the formability of 304L was diminished.

Conflict of interest

The authors declare that they have no conflict of interest.

References

1. X.R. Zhang, X.F. Liu, C.G. Yang, T. Xi, and K. Yang, New Strategy to Delay Food Spoilage: Application of New Food Contact Material with Antibacterial Function, *J. Mater. Sci. Technol. (Shenyang, China)*, 2021, **70**, p 59–66.
2. J.M. Zhan, H.Y. Bi, and M.C. Li, Thermal Fatigue Behavior of 441 Ferritic Stainless Steel in Air and Synthetic Automotive Exhaust Gas, *Sci. China (Technol. Sci.)*, 2022, **65**, p 169–178.
3. X.R. Zhang, C.G. Yang, and K. Yang, Contact-killing of Cu-bearing Stainless Steel Based on Charge Transfer Caused by Microdomain Potential Difference, *ACS Appl. Mater. Interfaces*, 2019, **12**, p 361–372.
4. Z.Y. Zhang, J.B. Tan, X.Q. Wu, E.H. Han, W. Ke, and J.C. Rao, Effects of Temperature on Corrosion Fatigue Behavior of 316LN Stainless Steel in High-temperature Pressurized Water, *Corros. Sci.*, 2019, **146**, p 80–89.
5. N.V. Doremalen, T. Bushmaker, D.H. Morris, M.G. Holbrook, and V.J. Munster, Aerosol and Surface Stability of SARS-COV-2 as Compared with SARS-COV-1, *N. Engl. J. Med.*, 2020, **382**, p 1564–1567.
6. L.T. Liu, A.W.H. Chin, P. Yu, L.L.M. Poon, and M.X. Huang, Anti-pathogen Stainless Steel Combating COVID-19, *Chem. Eng. J.*, 2021, **433**, p 133783.
7. P. Wang, Y.H. Yuan, K. Xu, H.S. Zhong, and X. Qi, Biological Applications of Copper-Containing Materials, *Bioact. Mater.*, 2021, **6**, p 916–927.
8. Z. Cao, J. Zhao, and K. Yang, Cu-Bearing Stainless Steel Reduces Cytotoxicity and Crystals Adhesion After Ureteral Epithelial Cells Exposing to Calcium Oxalate Monohydrate, *Sci. Reports*, 2018 https://doi.org/10.1038/s41598-018-32388-0
9. S. Curtze and V.T. Kuokkala, Dependence of Tensile Deformation Behavior of TWIP Steels on Stacking Fault Energy Temperature and Strain Rate, *Acta Mater.*, 2010, **58**, p 5129–5141.
10. X. Peng, D.Y. Zhu, Z.M. Hu, W.F. Yi, H.J. Liu, and M.J. Wang, Stacking Fault Energy and Tensile Deformation Behavior of High-Carbon Twinning-Induced Plasticity Steels: Effect of Cu Addition, *Mater. Des.*, 2013, **45**, p 518–523.
11. J.H. Choi, M.C. Jo, H. Lee, A. Zargaran, T. Song, S.S. Sohn, N.J. Kim, and S. Lee, Cu Addition Effects on TRIP to TWIP Transition and Tensile Property Improvement of Ultra-High-Strength Austenitic High-Mn Steels, *Acta Materialia*, 2019, **166**, p 246–260. https://doi.org/10.1016/j.actamat.2018.12.044
12. G. Singh, S.M. Hong, K. Oh-Ishi, K. Hono, E. Fleury and U. Ramamurty, Enhancing the High Temperature Plasticity of a Cu-containing Austenitic Stainless Steel through Grain Boundary Strengthening, *Mater. Sci. Eng. A*, 2014, **602**, p 77–88.
13. B.M. Gonzalez, C.S.B. Castro, V.T.L. Buono, J.M.C. Vilela, M.S. Andrade, J.M.D. Moraes, and M.J. Mantel, The Influence of Copper Addition on the Formability of AISI 304 L4L Stainless Steel, *Mater. Sci. Eng. A*, 2003, **343**, p 51–56.
14. I.T. Hong and C.H. Koo, Antibacterial Properties, Corrosion Resistance and Mechanical Properties of Cu-Modified SUS 304 L4L Stainless Steel, *Mater. Sci. Eng. A*, 2005, **393**, p 213–222.
15. S.J. Kim, C.G. Lee, T.H. Lee, and C.S. Oh, Effect of Cu, Cr and Ni on Mechanical Properties of 0.15 wt.% C TRIP-Aided Cold Rolled Steels, *Scr. Metall.*, 2003, **48**, p 539–544.
16. Z.B. Jiao, J.H. Luan, M.K. Miller, and C.T. Liu, Precipitation Mechanism and Mechanical Properties of an Ultra-High Strength Steel Hardened by Nanoscale NiAl and Cu Particles, *Acta Metall.*, 2015, **97**, p 58–67.
17. T. Xi, M.B. Shahzad, D.K. Xu, J.L. Zhao, C.G. Yang, M. Qi, and K. Yang, Copper Precipitation Behavior and Mechanical Properties of Cu-Bearing 316L Austenitic Stainless Steel: A Comprehensive Cross-Correlation Study, *Mater. Sci. Eng. A*, 2016, **675**, p 243–252.
18. K. Yang and M.Q. Lv, Antibacterial Properties of an Austenitic Antibacterial Stainless Steel and Its Security for Human Body, *Mater. Sci. Technol.*, 2007, **23**, p 49–52.
19. I. Sen, E. Amankwah, N.S. Kumar, E. Fleury, K. Oh-ishi, K. Hono, and U. Ramamurty, Microstructure and Mechanical Properties of Annealed SUS 304LH Austenitic Stainless Steel with Copper, *Mater. Sci. Eng. A*, 2011, **528**, p 4491–4499.
20. A.F. Padilha and P.R. Rios, Decomposition of Austenite in Austenitic Stainless Steels, *ISIJ Int.*, 2002, **42**, p 325–327.
21. J.X. Huang, Y.E. Xiao-Ning, and X.U. Zhou, Effect of Cold Rolling on Microstructure and Mechanical Properties of AISI 301LN Metastable Austenitic Stainless Steels, *J. Iron Steel Res. Int.*, 2012, **10**, p 59–63.
22. J.Y. Choi and W. Jin, Strain Induced Martensite Formation and Its Effect on Strain Hardening Behavior in the Cold Drawn 304 Austenitic Stainless Steels, *Scr. Mater.*, 1997, **36**, p 99–104.
23. L. Bracke, G. Mertens, J. Penning, B. Cooman, M. Liebeherr, and N. Akdut, Influence of Phase Transformations on the Mechanical Properties of High-strength Austenitic Fe-Mn-Cr Steel, *Metall. Trans. A*, 2006, **37**, p 307–317.
24. S. Curtze, V.-T. Kuokkala, A. Oikari, J. Talonen, and H. Hänninen, Thermodynamic Modeling of the Stacking Fault Energy of Austenitic steels, *Acta Mater.*, 2011, **59**, p 1068–1076.
25. J.A. Venables, The Nucleation and Propagation of Deformation Twins, *J. Phys. Chem. Solids*, 1964, **25**, p 693–700.
26. L.C.M. Gilapa, C.A.S.D. Oliveira, and M.R.D. Silva, Effect of Copper on the Formation of Strain-Induced Martensite in Two Austenitic Stainless Steels AISI 304, *Mater. Sci. Eng. A.*, 2015, **622**, p 212–218.
27. K. Nohara, Y. Ono, and N. Ohashi, Composition and Grain Size Dependence of Strain Induced Martensitic Transformation in Metastable Austenitic Stainless Steels, *Mater. Char.*, 1977, **63**, p 772–782.
28. K.K. Alaneme, S.M. Hong, I. Sen, E. Fleury, and U. Ramamurty, Effect of Copper Addition on the Fracture and Fatigue Crack Growth Behavior of Solution Heat-Treated SUS 304LH Austenitic Steel, *Mater. Sci. Eng. A.*, 2010, **527**, p 4600–4604.
29. J.Z. Shi, *Microstructure and Properties of Copper-bearing Antibacterial Austenite Stainless Steel*, Lanzhou University of Technology, Lanzhou, 2010
30. N. Gong and R.D.K. Misra, Favourable Modulation of Osteoblast Cellular Activity on Cu-Containing Austenitic Stainless Steel and Comparison with the Cu-Free Counterpart, *Mater. Technol.*, 2019, **35**, p 411–420.